Asian Journal of Green Chemistry 10 (2026) 601-627

Asian Journal of Green Chemistry

Original Research Article View Article Online | View Journal

Uncovering Antibacterial Agents in *Petiveria alliacea* through Computational and Experimental Methods

Jajang Japar Sodik[1,*], Entris Sutrisno[2], Dieni Mardliyani[3], Taufik Muhammad Fakih[3]

[1]*Department of Pharmaceutical and Medicinal Chemistry, Faculty of Pharmacy, Universitas Bhakti Kencana, Jl. Soekarno-Hatta Bandung 40614, Indonesia*
[2]*Department of Pharmacology and Clinical Pharmacy, Faculty of Pharmacy, Universitas Bhakti Kencana, Jl. Soekarno-Hatta Bandung 40614, Indonesia*
[3]*Department of Pharmacy, Faculty of Mathematics and Natural Sciences, Universitas Islam Bandung, Jl. Ranggagading 40116, Indonesia*

ARTICLE INFORMATION

Submitted: 2025-10-31
Revised: 2025-12-16
Accepted: 2026-01-26
Published: 2026-01-27
Manuscript ID: AJGC-2510-1857
DOI: 10.48309/ajgc.2026.556397.1857

KEYWORDS

Antibacterial candidate
Petiveria alliacea L.
Molecular dynamics simulation
Drug development

ABSTRACT

In response to the urgent need for innovative antibiotics, this study combined *in silico* and *in vitro* approaches to identify and evaluate novel bioactive compounds from *Petiveria alliacea* L. for their antibacterial potential. Through computational analysis, the derivatives exhibited strong binding affinities for key bacterial targets, including tyrosine phosphatase and FtsZ. Molecular dynamics (MD) simulations further validated the exceptional stability of these compounds during their interaction with the FtsZ protein, as evidenced by parameters such as root mean square deviation (RMSD), root mean square fluctuation (RMSF), radius of gyration (Rg), and solvent-accessible surface area (SASA). These findings align with the mechanisms of action of well-known antibiotics such as ciprofloxacin and griseofulvin, which target eukaryotic microtubules, whereas FtsZ serves as the prokaryotic counterpart. Complementing these computational findings, *in vitro* antibacterial activity testing revealed promising MIC and MBC values, confirming the ability of the bioactive compounds to inhibit and kill bacterial strains effectively. Collectively, the integration of computational and experimental approaches underscores the potential of bioactive compounds from *Petiveria alliacea* L. as effective antibacterial agents targeting the FtsZ protein. This study contributes to the development of novel antibiotics and provides a robust framework for future drug discovery efforts.

Corresponding author, E-mail: jajang.japar@bku.ac.id (J. J. Sodik)
Tel.: +6281332034440.

Graphical Abstract

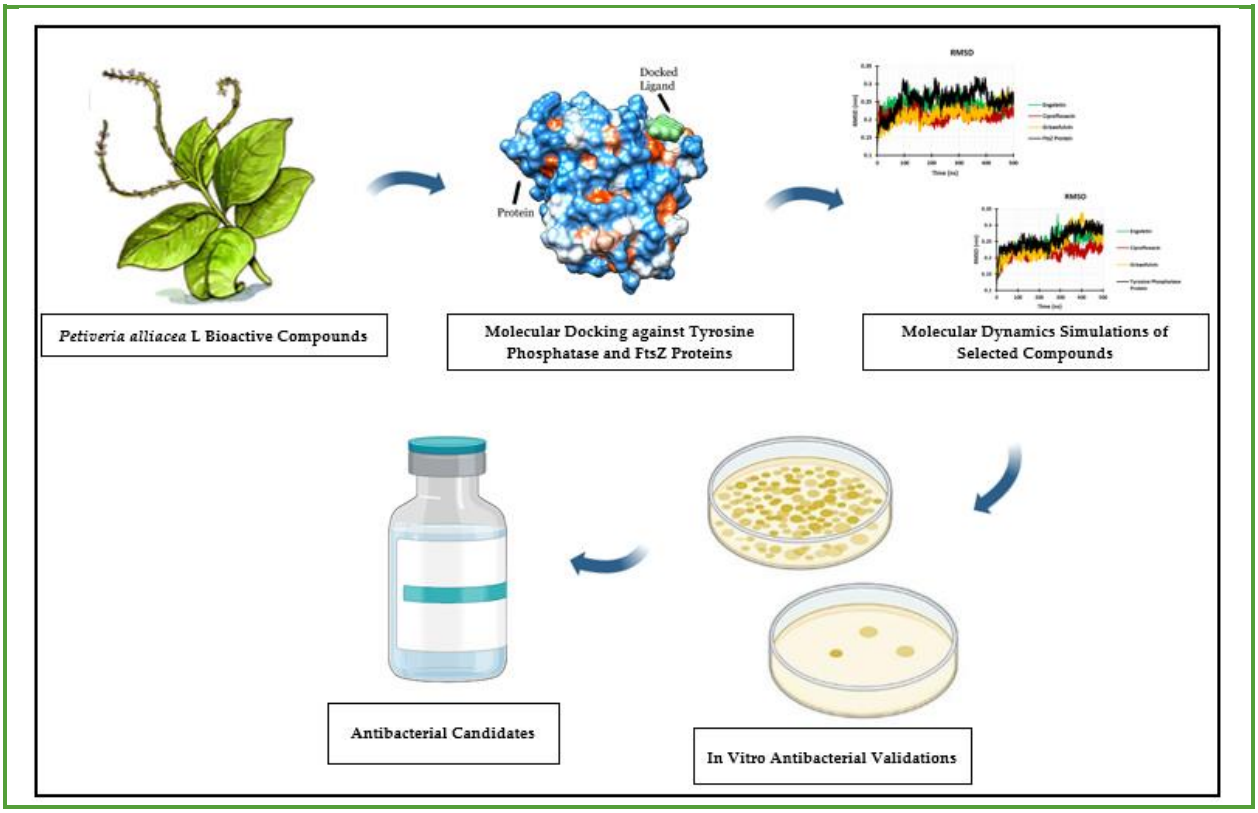

Introduction

A sharp rise in bacterial infections and growing antibiotic resistance now poses a major global health threat. After the antibiotic "golden age" which began with penicillin's discovery in 1928 and waned by the mid-1950s, new antibiotic development has slowed, contributing to today's antimicrobial resistance crisis [1,2]. While most natural antibiotics originate from filamentous actinomycetes, griseofulvin, first identified in *Penicillium griseofulvum* in 1939, remains a notable fungal secondary metabolite. It has since been found in multiple fungal species and shows therapeutic potential beyond dermatophyte infections, including activity against colon and breast cancer, hepatitis C virus, and possibly COVID-19 [3,4]. Ciprofloxacin, a widely active second-generation fluoroquinolone, was patented in 1980 and approved in 1987 [5]. Its strong pharmacokinetic profile and relatively low toxicity have made it useful against a broad range of bacterial infections, and the World Health Organization (WHO) classifies it as critically important in human medicine [6]. In 2019, it was the 113th most prescribed drug in the United States, with over five million prescriptions. However, like other antibiotics, bacterial resistance to ciprofloxacin has risen quickly, reducing its effectiveness. To address this, numerous ciprofloxacin derivatives have been developed to improve fluoroquinolone activity and counter resistance [7]. Over the past two decades, studies have validated many traditional uses of *Petiveria alliacea* L. (Phytolaccaceae) through animal experiments and neurobehavioral models [8]. Traditionally, the plant is linked to diuretic, analgesic, anti-inflammatory, antimicrobial, antirheumatic,

antileukemic, and other medicinal effects [9]. Phytochemical research has identified diverse metabolites, including sulfur compounds, flavonoids, and alkaloids, that can interact with biological systems and potential bacterial targets [10]. Nonetheless, the specific active compounds and mechanisms of action of *Petiveria alliacea* remain largely unclear. Due to its rich bioactive compounds, *Petiveria alliacea* L. has recently gained attention for its antibacterial potential. Ethanol leaf extracts have shown activity against various bacteria, including MSCNS, MRSA, MSSA, MRCNS, *Staphylococcus aureus*, *Pseudomonas aeruginosa*, *Bacillus subtilis*, *Bacillus cereus*, *Escherichia coli*, and VRE [11]. However, effects vary among strains, and the underlying molecular mechanisms remain poorly understood. With few new antibiotics developed in recent decades despite extensive screening of bacterial and fungal metabolites, there is an urgent need for more effective agents to address the global antimicrobial resistance crisis [12,13].

Theoretical studies play a crucial role in speeding drug development and saving resources, as shown by successful computational methods in medical research [14]. These approaches, from target identification to drug repurposing for multidrug-resistant infections, demonstrate flexibility and efficiency in tackling health challenges [15]. This study investigated the antibacterial potential of bioactive compounds from *Petiveria alliacea* L. using both *in silico* and *in vitro* methods. Computational analyses evaluated their binding affinity and stability against the bacterial FtsZ protein, essential for cell division and structurally similar to microtubules targeted by ciprofloxacin and griseofulvin [16]. *In vitro* assays confirmed these compounds' antibacterial activity through MIC and MBC values. Motivated by the urgent need for new antibiotics amid rising resistance, this work aims to identify effective antibacterial agents from *Petiveria alliacea* compounds, combining computational predictions with experimental validation to accelerate drug discovery and provide promising candidates against resistant bacteria.

Experimental

Designing bioactive compounds in Petiveria alliacea L.

In this research, molecular hybridization was applied to design new drug candidates by combining key pharmacophoric elements from bioactive compounds of *Petiveria alliacea* L. This strategy yielded innovative hybrid molecules with improved affinity and efficacy. The novelty of the synthesized compounds was evaluated using the Clarivate Analytics Integrity Drug Discovery Portal [17].

Preparation of receptors and bioactive compounds

The procedure was conducted by crafting the two-dimensional configurations of ligands through ChemDraw Professional 16.0 software. Subsequently, the three-dimensional molecular arrangements of these compounds were refined and optimized utilizing Chem3D 16.0 [18]. Ligand arrangement was executed via the LigPrep interface within Maestro [19]. For the receptors, the three-dimensional protein arrangements were sourced in .pdb format from the RCSB Protein Data Bank (PDB). The PDB IDs corresponding to the tyrosine phosphatase [20], filamenting temperature-sensitive mutant Z (FtsZ) [21], UDP-N-acetylglucosamine enolpyruvyl transferase (murA) [22], penicillin-binding protein 2 (PBP2) [23], DNA gyrase subunit B (GyrB) [24], DNA topoisomerase IV [25], and primase proteins [26]. These proteins are widely acknowledged as significant drug targets. All protein configurations underwent

preparation utilizing the Protein Preparation Wizard within Maestro.

Drug-like characteristics of the bioactive compounds

To assess the drug-likeness of the molecules, Lipinski's rule of five was applied—including criteria for molecular weight (<500 Da), hydrogen bond donors (≤5), hydrogen bond acceptors (≤10), and LogP (<5). Compliance with these parameters was evaluated using the SwissADME web tool, supporting their potential suitability for drug development.

Forecasts on biological activities of the bioactive compounds

Biological activity predictions for the designed derivatives were generated using the PASS Online tool available through the Way2Drug portal [27]. The predictions are based on structure–activity relationships derived from a diverse training set that includes approximately 7,000 antibacterial agents, with an estimated accuracy of 0.92. Compound structures were submitted as MOL files, and PASS provided probability of activity (Pa) values for each molecule.

Computational molecular docking studies

Molecular docking was performed using AutoDock Vina 1.2.3 and AutoDock Tools 4.2.6 [28,29]. Binding sites on target proteins were identified with CASTp 3.0, and a 20 Å grid box was defined around each predicted pocket [30]. Binding free energies were estimated using the MM-GBSA method [31]. Ligand–receptor interactions were visualized with Discovery Studio Visualizer v23 [32].

Computational molecular dynamics simulations

To validate the docking results, molecular dynamics (MD) simulations were performed using GROMACS 2016.3 with the AMBER99SB-ILDN force [33,34]. Proteins, reference drugs (ciprofloxacin and griseofulvin), and top protein–ligand complexes were simulated for 500 ns. Ligand parameters were generated with ACPYPE [35]**.** Systems were solvated with TIP3P water and neutralized with Na^+ and Cl^- ions. After energy minimization at 1,000 kJ/mol/nm, NVT and NPT equilibrations were run for 1 ns each at 310 K and 1 bar using the Nose–Hoover thermostat and Berendsen barostat. Trajectories were collected every 2 ps and analyzed for RMSD, RMSF, radius of gyration (Rg), and solvent-accessible surface area (SASA).

Computational binding free energy calculations using MM-PBSA

The study utilized the gmx_MMPBSA module within GROMACS 2016.3 to conduct molecular mechanics Poisson–Boltzmann surface area (MM-PBSA) analyses and investigate binding free energies [36]. The binding free energy (ΔGbind) was calculated using Equation 1:

$$\Delta G_{bind} = G_{complex} - (G_{protein} + G_{ligand}) \quad (1)$$

Here, ΔGbind represents the total binding energy of the complex, where Gcomplex signifies the binding energy of protein, and Gligand denotes the binding energy of the ligand.

In vitro antibacterial activity testing using the microdilution method

To validate the docking results, *in vitro* antibacterial assays were performed alongside MD simulations. Minimum Inhibitory Concentrations (MICs) were determined by assessing medium clarity after incubation,

identifying the lowest concentration of each selected compound that inhibited visible microbial growth. Minimum Bactericidal Concentrations (MBCs) were established by inoculating 5 µL from clear wells onto Nutrient Agar or Sabouraud Dextrose Agar and incubating at 37 °C for 24 hours; absence of colony growth indicated the MBC. The antibacterial and antifungal efficacy of the compounds was evaluated by comparing their MIC and MBC values with those of ciprofloxacin and fluconazole. Activity classification was based on the MBC/MIC ratio, where ≤4 denotes bactericidal or fungicidal action and >4 indicates bacteriostatic or fungistatic effects [37,38]. All tests were conducted in triplicate, with standard deviations calculated and appropriate controls included to ensure result reliability.

Results and Discussion

This study employed an integrated approach combining *in vitro* testing with molecular hybridization in drug design. Key pharmacophoric elements from bioactive compounds of *Petiveria alliacea* L. were combined to create hybrid molecules with enhanced affinity and efficacy. *In vitro* antibacterial assays validated the potential of these hybrids, providing experimental support for their effectiveness. This approach highlights the promise of natural products in drug discovery, offering novel candidates inspired by traditional medicinal plants. By integrating computational and experimental methods, the study demonstrates the value of leveraging natural resources to develop potent and reliable therapeutic agents.

Analyzing the structural characteristics of bioactive compounds

The MOL files of bioactive compounds, from *Petiveria alliacea* L. were used for similarity searches under default settings. None of the designed compounds showed resemblance to existing drugs in the Clarivate Analytics Integrity database. Table 1 presents the 2D structures of these novel compounds, along with their calculated LogP values and ligand bond characteristics. Molecular weights ranged from 226.42 to 504.70 g/mol, and predicted LogP values ranged from −2.54 to 7.79. Most compounds complied with Lipinski's rule of five, having no more than 10 hydrogen bond acceptors and 5 hydrogen bond donors, except for astilbin, engeletin, myricetin, and myricitrin. Despite some deviations, the applicability of Lipinski's rule for these bioactive compounds should be reconsidered.

Table 1. 2D Structures and Lipinski analysis of *Petiveria alliacea* l. bioactive compounds

Phytochemical name	Two-dimensional structure	Analysis according to Lipinski's rule
3-Epiilexgenin-A	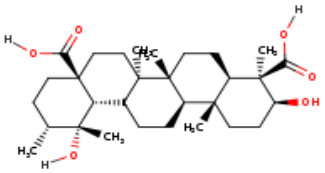	Molecular weight: 504.70 g/mol Lipophilicity: 4.49 Hydrogen bond acceptors: 6 Hydrogen bond donors: 4 Violations: Yes; 1 violation: MW>500
5-*O*-Methylether-(5-*O*-methylleridol)	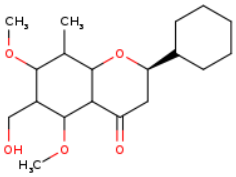	Molecular weight: 340.45 g/mol Lipophilicity: 2.25 Hydrogen bond acceptors: 5 Hydrogen bond donors: 1 Violations: Yes; 0 violation

Phytochemical name	Two-dimensional structure	Analysis according to Lipinski's rule
6-Formyl-8-methyl-7-*0*-methylpinocembrin	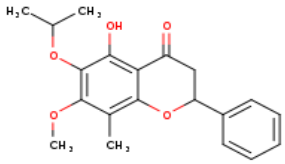	Molecular weight: 342.39 g/mol Lipophilicity: 3.55 Hydrogen bond acceptors: 5 Hydrogen bond donors: 1 Violations: Yes; 0 violation
6-Hydroxymethyl-7-*0*-methylpinocembrin (leridol)	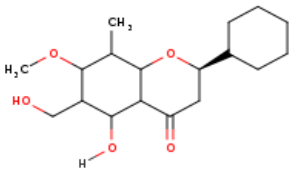	Molecular weight: 326.43 g/mol Lipophilicity: 1.73 Hydrogen bond acceptors: 5 Hydrogen bond donors: 2 Violations: Yes; 0 violation
Alpha-friedelinol	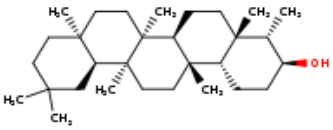	Molecular weight: 428.73 g/mol Lipophilicity: 7.38 Hydrogen bond acceptors: 1 Hydrogen bond donors: 1 Violations: Yes; 1 violation: MLOGP>4.15
Astilbin	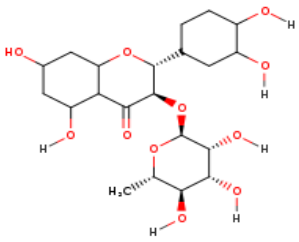	Molecular weight: 462.49 g/mol Lipophilicity: −1.86 Hydrogen bond acceptors: 11 Hydrogen bond donors: 7 Violations: No; 2 violations: NorO>10, NHorOH>5
Babinervic-acid	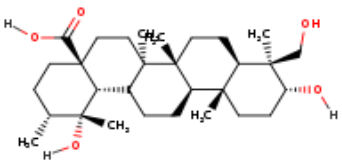	Molecular weight: 490.72 g/mol Lipophilicity: 4.80 Hydrogen bond acceptors: 5 Hydrogen bond donors: 4 Violations: Yes; 1 violation: MLOGP>4.15
Beta-sitosterol	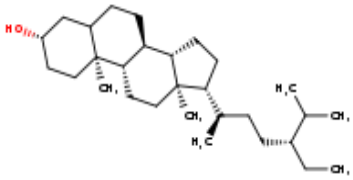	Molecular weight: 416.72 g/mol Lipophilicity: 7.10 Hydrogen bond acceptors: 1 Hydrogen bond donors: 1 Violations: Yes; 1 violation: MLOGP>4.15
Di(benzyltrithio)-methane		Molecular weight: 400.77 g/mol Lipophilicity: 5.96 Hydrogen bond acceptors: 0 Hydrogen bond donors: 0 Violations: Yes; 1 violation: MLOGP>4.15
Dibenzyl-disulphide	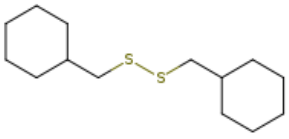	Molecular weight: 258.49 g/mol Lipophilicity: 4.83 Hydrogen bond acceptors: 0 Hydrogen bond donors: 0 Violations: Yes; 1 violation: MLOGP>4.15

Phytochemical name	Two-dimensional structure	Analysis according to Lipinski's rule
Dibenzyl-sulphide	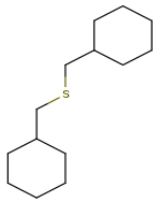	Molecular weight: 226.42 g/mol Lipophilicity: 4.63 Hydrogen bond acceptors: 0 Hydrogen bond donors: 0 Violations: Yes; 1 violation: MLOGP>4.15
Dibenzyl-tetrasulphide	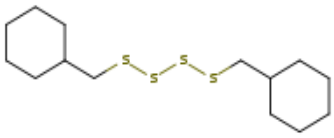	Molecular weight: 322.62 g/mol Lipophilicity: 5.31 Hydrogen bond acceptors: 0 Hydrogen bond donors: 0 Violations: Yes; 1 violation: MLOGP>4.15
Dibenzyl-trisulphide	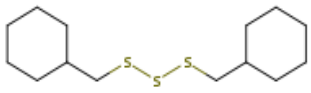	Molecular weight: 290.55 g/mol Lipophilicity: 5.08 Hydrogen bond acceptors: 0 Hydrogen bond donors: 0 Violations: Yes; 1 violation: MLOGP>4.15
Dihydro-kaempferol	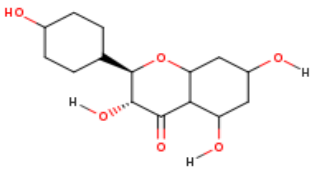	Molecular weight: 300.35 g/mol Lipophilicity: −0.18 Hydrogen bond acceptors: 6 Hydrogen bond donors: 4 Violations: Yes; 0 violation
Dihydroquercetin	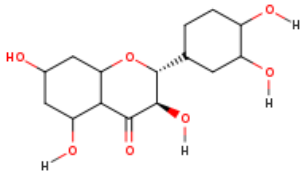	Molecular weight: 316.35 g/mol Lipophilicity: −0.88 Hydrogen bond acceptors: 7 Hydrogen bond donors: 5 Violations: Yes; 0 violation
Engeletin	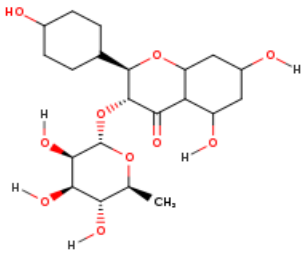	Molecular weight: 446.49 g/mol Lipophilicity: −1.15 Hydrogen bond acceptors: 10 Hydrogen bond donors: 6 Violations: Yes; 1 violation: NHorOH>5
Isoarborinol-acetate	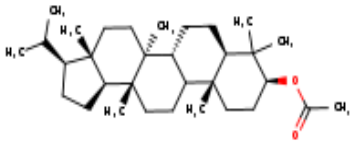	Molecular weight: 470.77 g/mol Lipophilicity: 7.79 Hydrogen bond acceptors: 2 Hydrogen bond donors: 0 Violations: Yes; 1 violation: MLOGP>4.15
Isoarborinol	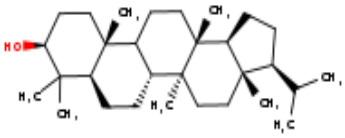	Molecular weight: 428.73 g/mol Lipophilicity: 7.36 Hydrogen bond acceptors: 1 Hydrogen bond donors: 1 Violations: Yes; 1 violation: MLOGP>4.15
Leridal-chalcone	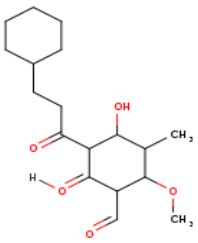	Molecular weight: 325.42 g/mol Lipophilicity: −0.44 Hydrogen bond acceptors: 5 Hydrogen bond donors: 2 Violations: Yes; 0 violation

Phytochemical name	Two-dimensional structure	Analysis according to Lipinski's rule
Myricetin	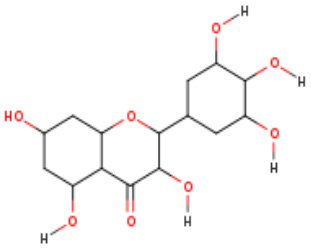	Molecular weight: 332.35 g/mol Lipophilicity: −1.73 Hydrogen bond acceptors: 8 Hydrogen bond donors: 6 Violations: Yes; 1 violation: NHorOH>5
Myricitrin	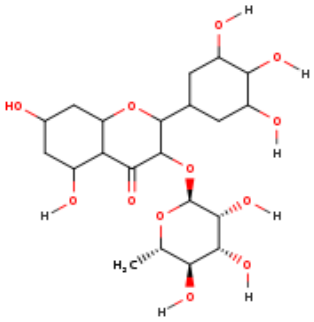	Molecular weight: 478.49 g/mol Lipophilicity: −2.54 Hydrogen bond acceptors: 12 Hydrogen bond donors: 8 Violations: No; 2 violations: NorO>10, NHorOH>5
Petiveral-4-ethyl	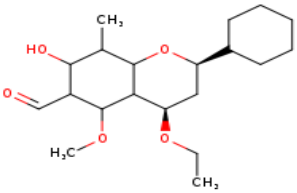	Molecular weight: 354.48 g/mol Lipophilicity: 2.43 Hydrogen bond acceptors: 5 Hydrogen bond donors: 1 Violations: Yes; 0 violation
Petiveral	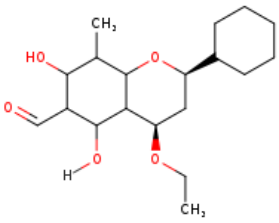	Molecular weight: 340.45 g/mol Lipophilicity: 2.12 Hydrogen bond acceptors: 5 Hydrogen bond donors: 2 Violations: Yes; 0 violation
S-Benzyl-phenylmethane-thiosulphinate	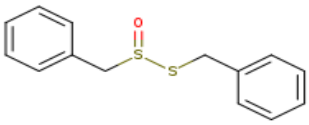	Molecular weight: 262.39 g/mol Lipophilicity: 3.22 Hydrogen bond acceptors: 1 Hydrogen bond donors: 0 Violations: Yes; 0 violation
Ciprofloxacin	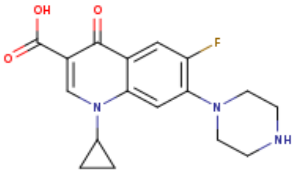	Molecular weight: 331.34 g/mol Lipophilicity: 1.10 Hydrogen bond acceptors: 5 Hydrogen bond donors: 2 Violations: Yes; 0 violation
Griseofulvin	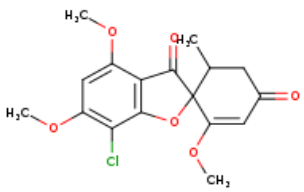	Molecular weight: 352.77 g/mol Lipophilicity: 2.41 Hydrogen bond acceptors: 6 Hydrogen bond donors: 0 Violations: Yes; 0 violation

To assess the antibacterial potential of the designed bioactive compounds, an *in silico* approach was employed combining molecular docking, molecular dynamics, and PASS (Prediction of Activity Spectra for Substances). PASS analyzes structure–activity relationships across over 250,000 compounds, with an overall prediction accuracy of approximately 95%. Table 2 summarizes the predicted biological activities, highlighting antibacterial effects and phosphatase inhibition. Ciprofloxacin and griseofulvin served as benchmark drugs. Several bioactive compounds showed antibacterial activity surpassing the controls, and all exhibited significant potential as phosphatase inhibitors, warranting further investigation.

Table 2. Predicted antibacterial and phosphatase inhibitory activities of *Petiveria alliacea* l. compounds (Pa)

Phytochemical name	Two-dimensional structure	Antibacterial activity (Pa)	Phospatase inhibitor activity (Pa)
3-Epiilexgenin-A	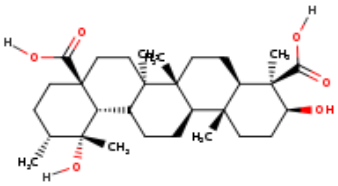	0.289	0.720
5-*O*-Methylether-(5-*O*-methylleridol)	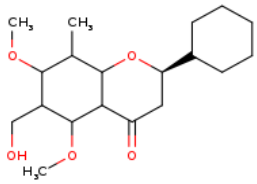	0.309	0.593
6-Formyl-8-methyl-7-*0*-methylpinocembrin	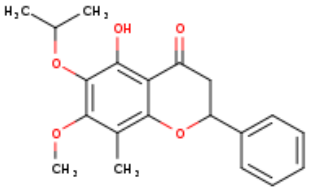	0.385	0.482
6-Hydroxymethyl-7-*0*-methylpinocembrin (leridol)	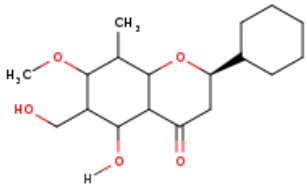	0.390	0.655
Alpha-friedelinol	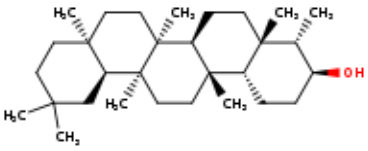	0.351	0.676

Phytochemical name	Two-dimensional structure	Antibacterial activity (Pa)	Phospatase inhibitor activity (Pa)
Astilbin	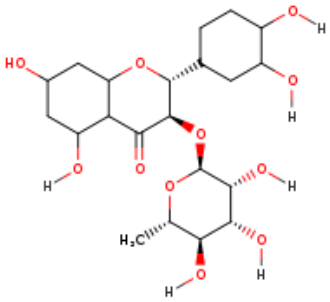	0.618	0.563
Babinervic-acid	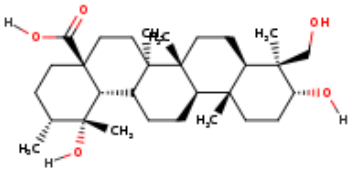	0.356	0.722
Beta-sitosterol	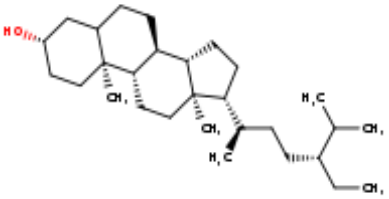	0.283	0.563
Di(benzyltrithio)-methane	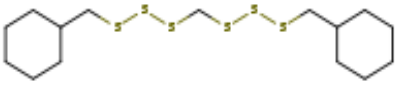	0.352	0.252
Dibenzyl-disulphide	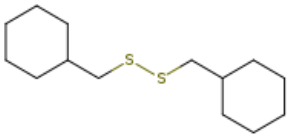	0.295	0.339
Dibenzyl-sulphide	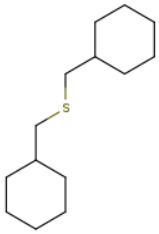	0.302	0.503
Dibenzyl-tetrasulphide	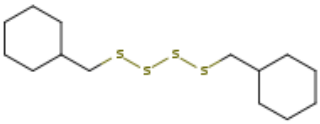	0.211	0.289
Dibenzyl-trisulphide	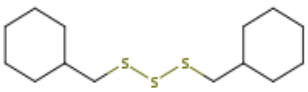	0.304	0.289
Dihydro-kaempferol	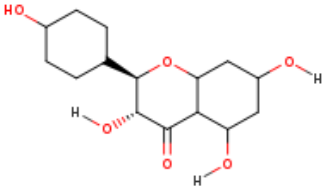	0.384	0.653

Phytochemical name	Two-dimensional structure	Antibacterial activity (Pa)	Phospatase inhibitor activity (Pa)
Dihydroquercetin	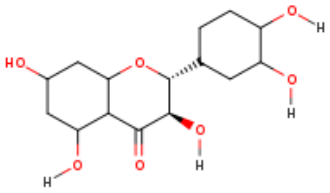	0.382	0.627
Engeletin	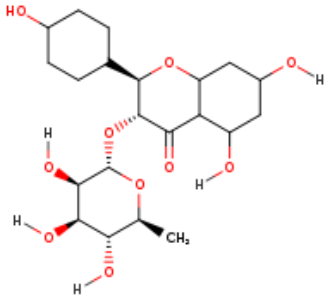	0.619	0.290
Isoarborinol-acetate	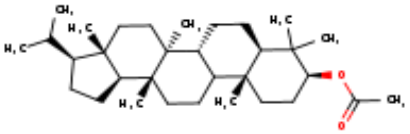	0.240	0.726
Isoarborinol	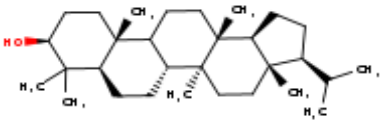	0.234	0.770
Leridal-chalcone	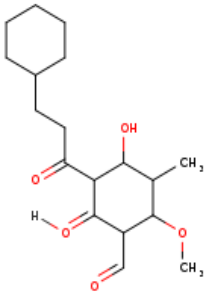	0.442	0.673
Myricetin	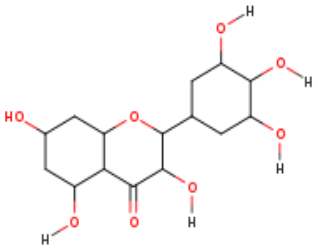	0.421	0.454

Phytochemical name	Two-dimensional structure	Antibacterial activity (Pa)	Phospatase inhibitor activity (Pa)
Myricitrin	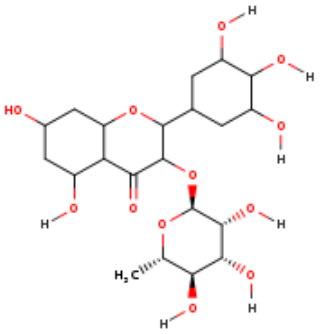	0.662	0.494
Petiveral-4-ethyl	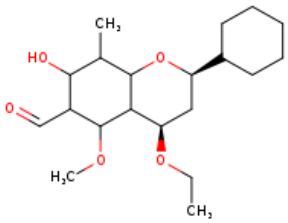	0.475	0.671
Petiveral	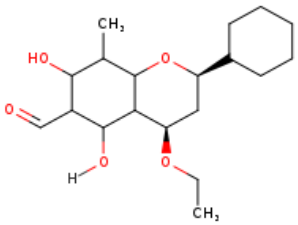	0.524	0.725
S-benzyl-phenylmethane-thiosulphinate	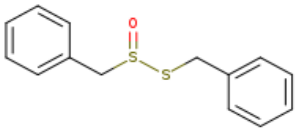	0.337	0.289
Ciprofloxacin	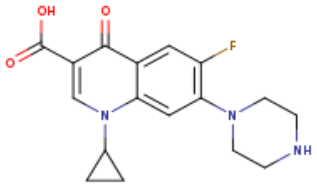	0.588	0.301
Griseofulvin	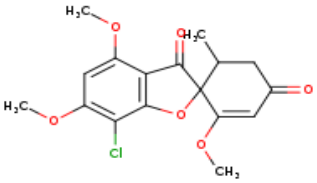	0.337	0.803

Computational molecular docking studies

The potential of bioactive compounds from *Petiveria alliacea* L. was investigated against a key bacterial protein tyrosine phosphatase (PTP), a virulence factor in pathogens such as *Mycobacterium tuberculosis*, *Staphylococcus aureus*, *Salmonella typhimurium*, and *Yersinia* sp. In *Pseudomonas aeruginosa*, tyrosine phosphatase A (TbpA) promotes biofilm formation by modulating c-di-GMP levels [39]**.** In this study, engeletin showed a binding affinity to TbpA comparable to ciprofloxacin (−7.4 kcal/mol), while 3-epiilexgenin-A and astilbin exhibited stronger binding than griseofulvin

(−7.2 kcal/mol). These results align with predictions from Way2Drug. FtsZ, the bacterial homolog of eukaryotic tubulin, forms the Z-ring at midcell to regulate cytokinesis [40]. It is a prime antibacterial target due to its essential role in bacterial division and low sequence similarity (10–18%) to eukaryotic tubulin, minimizing host toxicity [41]. Docking analysis at the interdomain cleft revealed strong binding of *Petiveria alliacea* L. compounds, notably astilbin (−9.1 kcal/mol), dihydrokaempferol (−9.0 kcal/mol), and engeletin (−9.3 kcal/mol), exceeding reference drugs ciprofloxacin and griseofulvin. MurA, which initiates peptidoglycan synthesis, is another key antibacterial target. Astilbin, dihydroquercetin, and myricitrin showed the highest affinities, while ciprofloxacin and griseofulvin displayed negligible binding [42]. Ciprofloxacin, a fluoroquinolone inhibiting DNA gyrase and topoisomerase IV, had a binding energy of −8.0 kcal/mol to GyrB, whereas 3-epiilexgenin-A (−9.8 kcal/mol), alpha-friedelinol (−9.9 kcal/mol), and astilbin (−9.6 kcal/mol) showed stronger affinities. For DNA topoIV, astilbin (−7.7 kcal/mol), beta-sitosterol (−7.6 kcal/mol), and myricitrin (−8.0 kcal/mol) also outperformed the reference drugs. Overall, the designed bioactive compounds exhibited superior binding across multiple bacterial targets compared to ciprofloxacin and griseofulvin. To initiate the replication process of DNA, living organisms depend on a specific enzyme known as primase, which is responsible for synthesizing RNA primers. This study identified compounds targeting key bacterial enzymes. Alpha-friedelinol, isoarborinol acetate, and isoarborinol showed the strongest affinities for primase, with binding energies of −8.6, −8.4, and −8.5 kcal/mol, respectively, whereas griseofulvin and ciprofloxacin exhibited weaker binding (−6.8 and −7.5 kcal/mol). Penicillin-binding proteins (PBPs), crucial for cell wall peptidoglycan synthesis, were also targeted, with PBP2 showing the highest affinities. Astilbin, dihydroquercetin, and myricetin demonstrated strong binding energies of −8.4, −8.6, and −8.5 kcal/mol, surpassing other bioactive compounds (−4.1 to −8.2 kcal/mol). Binding affinities of all compounds from *Petiveria alliacea* L., compared to controls ciprofloxacin and griseofulvin, are summarized in Table 3.

Table 3. Binding energies of *Petiveria alliacea* l. compounds to bacterial targets (kcal/mol)

Target receptor	Phytochemical name	Binding affinity (kcal/mol)
Tyrosine phosphatase (4R0T)	**3-Epiilexgenin-A**	**−7.2**
	5-*O*-Methylether-(5-*O*-methylleridol)	−5.6
	6-Formyl-8-methyl-7-*0*-methylpinocembrin	−6.2
	6-Hydroxymethyl-7-*0*-methylpinocembrin (leridol)	−6.1
	Alpha-friedelinol	−7.1
	Astilbin	**−7.2**
	Babinervic-acid	−7.1
	Beta-sitosterol	−5.9
	Di(benzyltrithio)-methane	−4.6
	Dibenzyl-disulphide	−4.2
	Dibenzyl-sulphide	−4.7
	Dibenzyl-tetrasulphide	−3.8
	Dibenzyl-trisulphide	−4.3
	Dihydro-kaempferol	−6.3

Target receptor	Phytochemical name	Binding affinity (kcal/mol)
FtsZ (3VOB)	Dihydroquercetin	−7.0
	Engeletin	**−7.4**
	Isoarborinol-acetate	−6.9
	Isoarborinol	−7.0
	Leridal-chalcone	−5.5
	Myricetin	−7.0
	Myricitrin	−7.1
	Petiveral-4-ethyl	−6.1
	Petiveral	−6.1
	S-Benzyl-phenylmethane-thiosulphinate	−3.9
	Ciprofloxacin	−7.4
	Griseofulvin	−6.2
	3-Epiilexgenin-A	−8.5
	5-*O*-Methylether-(5-*O*-methylleridol)	−8.1
	6-Formyl-8-methyl-7-*0*-methylpinocembrin	−7.8
	6-Hydroxymethyl-7-0-methylpinocembrin (leridol)	−8.1
	Alpha-friedelinol	−8.4
	Astilbin	**−9.1**
	Babinervic-acid	−8.5
	Beta-sitosterol	−7.9
	Di(benzyltrithio)-methane	−6.6
	Dibenzyl-disulphide	−5.5
	Dibenzyl-sulphide	−5.2
	Dibenzyl-tetrasulphide	−5.4
	Dibenzyl-trisulphide	−5.8
MurA (1UAE)	**Dihydro-kaempferol**	**−9.0**
	Dihydroquercetin	−8.8
	Engeletin	**−9.3**
	Isoarborinol-acetate	−8.3
	Isoarborinol	−8.2
	Leridal-chalcone	−7.8
	Myricetin	−8.8
	Myricitrin	−8.5
	Petiveral-4-ethyl	−8.4
	Petiveral	−7.5
	S-Benzyl-phenylmethane-thiosulphinate	−5.4
	Ciprofloxacin	−8.2
	Griseofulvin	−7.8
	3-Epiilexgenin-A	−4.4
	5-*O*-Methylether-(5-*O*-methylleridol)	−8.4
	6-Formyl-8-methyl-7-*0*-methylpinocembrin	−8.8
	6-Hydroxymethyl-7-0-methylpinocembrin (leridol)	−7.0
	Alpha-friedelinol	−7.7
	Astilbin	**−9.5**
	Babinervic-acid	−7.3
	Beta-sitosterol	−6.5
	Di(benzyltrithio)-methane	−6.0
	Dibenzyl-disulphide	−6.7

Target receptor	Phytochemical name	Binding affinity (kcal/mol)
PBP2 (1MWT)	Dibenzyl-sulphide	−6.4
	Dibenzyl-tetrasulphide	−5.9
	Dibenzyl-trisulphide	−7.1
	Dihydro-kaempferol	−8.9
	Dihydroquercetin	**−9.1**
	Engeletin	−7.1
	Isoarborinol-acetate	−8.0
	Isoarborinol	−8.8
	Leridal-chalcone	−7.4
	Myricetin	−8.9
	Myricitrin	**−9.8**
	Petiveral-4-ethyl	−6.9
	Petiveral	−8.2
	S-Benzyl-phenylmethane-thiosulphinate	−4.4
	Ciprofloxacin	−6.7
	Griseofulvin	−6.1
	3-Epiilexgenin-A	−7.2
	5-*O*-Methylether-(5-O-methylleridol)	−7.1
	6-Formyl-8-methyl-7-*0*-methylpinocembrin	−7.2
	6-Hydroxymethyl-7-*0*-methylpinocembrin (leridol)	−6.2
	Alpha-friedelinol	−7.3
	Astilbin	**−8.4**
GyrB (4PRV)	Babinervic-acid	−6.6
	Beta-sitosterol	−6.8
	Di(benzyltrithio)-methane	−4.1
	Dibenzyl-disulphide	−4.5
	Dibenzyl-sulphide	−5.9
	Dibenzyl-tetrasulphide	−5.1
	Dibenzyl-trisulphide	−5.8
	Dihydro-kaempferol	−8.0
	Dihydroquercetin	**−8.6**
	Engeletin	−8.2
	Isoarborinol-acetate	−6.9
	Isoarborinol	−6.9
	Leridal-chalcone	−7.4
	Myricetin	**−8.5**
	Myricitrin	−8.1
	Petiveral-4-ethyl	−6.1
	Petiveral	−6.1
	S-Benzyl-phenylmethane-thiosulphinate	−6.4
	Ciprofloxacin	−6.2
	Griseofulvin	−5.6
	3-Epiilexgenin-A	**−9.8**
	5-*O*-Methylether-(5-*O*-methylleridol)	−8.5
	6-Formyl-8-methyl-7-*0*-methylpinocembrin	−8.6
	6-Hydroxymethyl-7-*0*-methylpinocembrin (leridol)	−8.9
	Alpha-friedelinol	**−9.9**
	Astilbin	**−9.6**

Target receptor	Phytochemical name	Binding affinity (kcal/mol)
	Babinervic-acid	−9.3
	Beta-sitosterol	−9.0
	Di(benzyltrithio)-methane	−5.7
	Dibenzyl-disulphide	−7.5
	Dibenzyl-sulphide	−6.8
	Dibenzyl-tetrasulphide	−6.1
	Dibenzyl-trisulphide	−7.4
	Dihydro-kaempferol	−8.5
	Dihydroquercetin	−8.9
	Engeletin	−9.0
	Isoarborinol-acetate	−9.1
	Isoarborinol	−9.5
	Leridal-chalcone	−7.9
	Myricetin	−8.8
	Myricitrin	−9.5
	Petiveral-4-ethyl	−8.7
	Petiveral	−8.5
	S-Benzyl-phenylmethane-thiosulphinate	−6.1
	Ciprofloxacin	−8.0
	Griseofulvin	−7.8
	3-Epiilexgenin-A	−7.3
	5-*O*-Methylether-(5-*O*-methylleridol)	−6.6
	6-Formyl-8-methyl-7-*0*-methylpinocembrin	−7.1
	6-Hydroxymethyl-7-0-methylpinocembrin (leridol)	−6.8
	Alpha-friedelinol	−7.5
DNA topoIV (1S14)	**Astilbin**	**−7.7**
	Babinervic-acid	−7.3
	Beta-sitosterol	**−7.6**
	Di(benzyltrithio)-methane	−5.3
	Dibenzyl-disulphide	−4.2
	Dibenzyl-sulphide	−4.8
	Dibenzyl-tetrasulphide	−3.8
	Dibenzyl-trisulphide	−4.4
	Dihydro-kaempferol	−7.0
	Dihydroquercetin	−7.3
	Engeletin	−7.0
	Isoarborinol-acetate	−7.0
	Isoarborinol	−7.2
	Leridal-chalcone	−6.3
	Myricetin	−7.5
	Myricitrin	**−8.0**
	Petiveral-4-ethyl	−6.2
	Petiveral	−6.4
	S-Benzyl-phenylmethane-thiosulphinate	−4.4
	Ciprofloxacin	−7.1
	Griseofulvin	−6.3
	3-Epiilexgenin-A	−7.8
Primase (1DDE)	5-*O*-Methylether-(5-*O*-methylleridol)	−7.3

Target receptor	Phytochemical name	Binding affinity (kcal/mol)
	6-Formyl-8-methyl-7-*0*-methylpinocembrin	−7.3
	6-Hydroxymethyl-7-*0*-methylpinocembrin (leridol)	−7.3
	Alpha-friedelinol	**−8.6**
	Astilbin	−7.7
	Babinervic-acid	−7.6
	Beta-sitosterol	−7.4
	Di(benzyltrithio)-methane	−6.4
	Dibenzyl-disulphide	−5.6
	Dibenzyl-sulphide	−5.6
	Dibenzyl-tetrasulphide	−5.3
	Dibenzyl-trisulphide	−6.2
	Dihydro-kaempferol	−7.1
	Dihydroquercetin	−7.2
	Engeletin	−7.8
	Isoarborinol-acetate	**−8.4**
	Isoarborinol	**−8.5**
	Leridal-chalcone	−7.5
	Myricetin	−7.0
	Myricitrin	−7.8
	Petiveral-4-ethyl	−6.5
	Petiveral	−6.8
	S-Benzyl-phenylmethane-thiosulphinate	−5.8
	Ciprofloxacin	−7.5
	Griseofulvin	−6.8

Table 4. Binding energies (kcal/mol) and inhibition constants of the most potent antibacterial compounds

Target receptor	Phytochemical name	Binding affinity (kcal/mol)	Inhibition constant
Tyrosine phosphatase (4R0T)	3-Epiilexgenin-A	−5.41	107.57 uM
	Astilbin	−8.35	758.35 nM
	Engeletin	**−8.77**	**372.15 nM**
	Ciprofloxacin	−7.12	6.02 uM
	Griseofulvin	−6.39	20.61 uM
FtsZ (3VOB)	Astilbin	−9.23	172.92 nM
	Dihydro-Kaempferol	−7.94	1.51 uM
	Engeletin	**−9.62**	**89.36 nM**
	Ciprofloxacin	−7.53	3.03 uM
	Griseofulvin	−5.71	65.23 uM
murA (1UAE)	Astilbin	−8.68	430.72 nM
	Dihydroquercetin	−7.29	4.54 uM
	Myricitrin	**−8.72**	**405.93 nM**
	Ciprofloxacin	−9.12	208.07 nM
	Griseofulvin	−7.36	4.01 uM
PBP2 (1MWT)	Astilbin	−6.56	15.58 uM
	Dihydroquercetin	−7.34	4.19 uM

Target receptor	Phytochemical name	Binding affinity (kcal/mol)	Inhibition constant
GyrB (4PRV)	**Myricetin**	**−6.63**	**13.84 uM**
	Ciprofloxacin	−6.62	14.01 uM
	Griseofulvin	−6.82	9.95 uM
	3-Epiilexgenin-A	−3.91	1.36 mM
	Alpha-friedelinol	−6.30	24.26 uM
	Astilbin	**−8.42**	**673.13 nM**
	Ciprofloxacin	−7.87	1.71 uM
	Griseofulvin	−8.21	955.85 nM
	Astilbin	−6.08	35.11 uM
DNA topoIV (1S14)	**Beta-sitosterol**	**−8.86**	**321.90 nM**
	Myricitrin	−6.58	15.14 uM
	Ciprofloxacin	−6.82	10.00 uM
	Griseofulvin	−6.36	21.87 uM
	Alpha-friedelinol	−7.70	2.28 uM
Primase (1DDE)	**Isoarborinol-Acetate**	**−8.90**	**300.44 nM**
	Isoarborinol	−8.71	411.82 nM
	Ciprofloxacin	−8.32	802.04 nM
	Griseofulvin	−6.31	23.74 uM

Table 5. Docking of *Petiveria alliacea* L. compounds against antibacterial targets

Target receptor	Phytochemical name	Hydrogen bond	Hydrophobic interaction	Electrostatic interaction	2D visualization
Tyrosine Phosphatase (4R0T)	Engeletin	ALA104:HN SER132: HG HIS134:HD1 GLY135:HN ARG138: HE ARG138:HH21 ASN136:OD1 ASN136:OD1 ASP171:OD2 ASP172:OD1 ASP105:OD1 HIS103:CA	ASP172:C,O MET173:N LYS133 HIS134 ALA104	ASP175:OD2	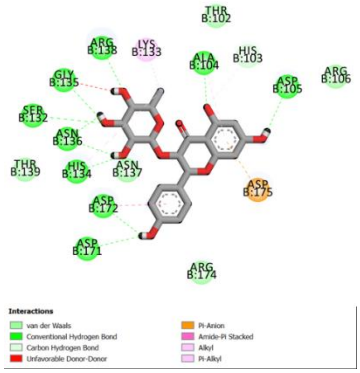
FtsZ (3VOB)	Engeletin	LEU209:HN THR265:HG1 ASP199:OD2 VAL207:O	VAL297:CG2 ILE228 LEU200 LEU209 LEU200		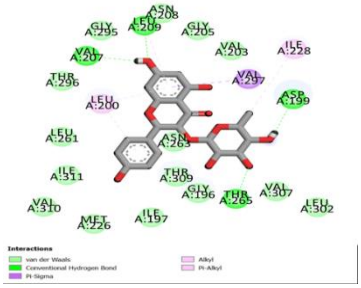

Target receptor	Phytochemical name	Hydrogen bond	Hydrophobic interaction	Electrostatic interaction	2D visualization
murA (1UAE)	Myricitrin	THR326:O THR326:O SER162: OG ASP123:OD1 ASP123: N LEU124: N LYS160:NZ SER162: OG	LEU124:CD1 VAL163 LYS160 VAL327		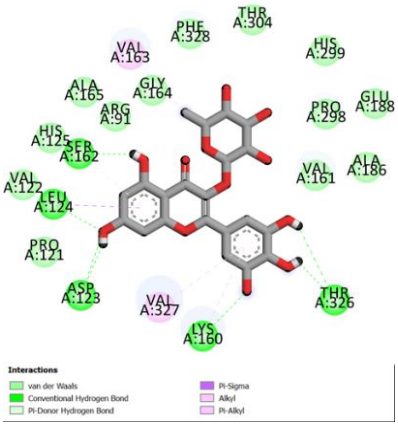
PBP2 (1MWT)	Myricetin	GLU447: N THR600:OG1 ALA642: N SER643: N SER643: OG ASN464:OD1 SER462:O SER462:O THR600:OG1 GLY640:O	TYR446 HIS583 MET641 ALA642 MET641		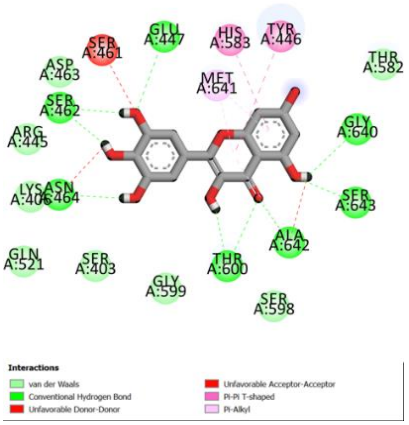
GyrB (4PRV)	Astilbin	ASN46:ND2 TYR109: OH ASP73:OD2 ASN46:O GLU50:OE1 GLY102:O ILE78:CA TYR109: OH	ILE94:CG2 TYR109 PRO79 VAL120		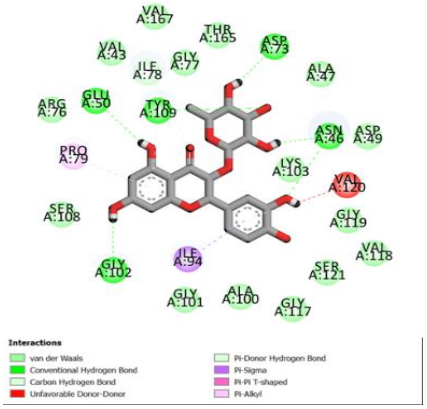

Target receptor	Phytochemical name	Hydrogen bond	Hydrophobic interaction	Electrostatic interaction	2D visualization
DNA topoIV (1S14)	Beta-sitosterol		ARG1072 MET1074 PRO1075 MET1074 PRO1075 MET1074 LEU1091 VAL1165 VAL1039 VAL1119 VAL1165 VAL1039 VAL1165		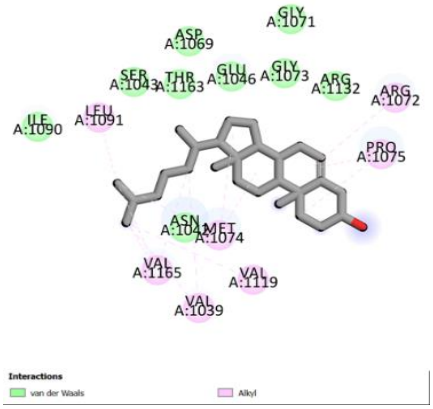
Primase (1DDE)	Isoarborinol-acetate	ASP345:OD2	TYR267 MET268 MET268 ALA283 MET268 LEU285 LEU285 TYR230 TYR230 TYR230 TYR230 TYR230 TYR230 TYR267 TYR267 TYR267		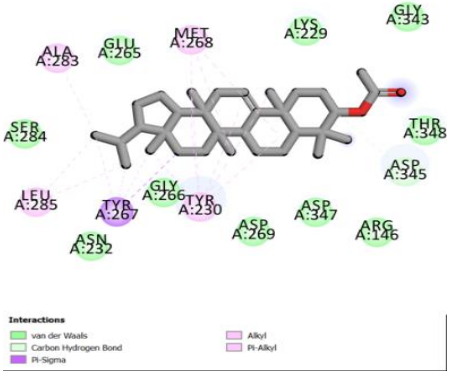

Molecular docking using AutoDock Tools 4.2.6 examined hydrogen bonding, hydrophobic, and electrostatic interactions of high-affinity compounds from *Petiveria alliacea* L. with antibacterial targets, as shown in Table 4. Only a few compounds showed optimal interactions with multiple targets: engeletin with tyrosine phosphatase and FtsZ, myricitrin with MurA, myricetin with PBP2, astilbin with GyrB, β-sitosterol with DNA topoIV, and isoarborinol-acetate with primase as shown in Table 5. These six compounds displayed stronger affinities than ciprofloxacin and griseofulvin. Notably, engeletin formed 18 molecular interactions with tyrosine phosphatase, including 12 hydrogen bonds, five hydrophobic contacts, and one electrostatic interaction.

Computational molecular dynamics simulations

The top two docked complexes underwent a 500 ns MD simulation to explore protein structural stability and conformational changes (tyrosine phosphatase + engeletin and FtsZ + engeletin). It is noteworthy that all bioactive compounds exhibited the strongest binding

affinity with MurA, PBP2, GyrB, DNA topoIV, and primase. The molecular docking analysis of tyrosine phosphatase aligns with PASS's biological activity prediction. The engeletin compound, identified through PASS, has a Pa value indicating antibacterial activity of 0.619. Subsequently, following Lipinski's rules, the compound qualifies as a drug candidate. Previous studies demonstrated engeletin's potent inhibition of CYP3A4 and CYP2D6, with IC_{50} values of 1.32 μM and 2.87 μM, respectively. CYP3A4 and CYP2D6, members of the CYP450 family, play significant roles in over 50% and 25% of clinical drug metabolism, respectively [43]**.** Moreover, engeletin, a bioactive compound, exhibited favorable binding to FtsZ, a microtubule homolog, potentially targeted by griseofulvin. Simulation trajectory files were scrutinized for RMSD, RMSF, Rg, and SASA.

Structural changes in FtsZ (3VOB)

Molecular dynamics simulations were utilized to explore the interaction between protein tyrosine phosphatase and bioactive compounds derived from *Petiveria alliacea* L. The stability of these complexes was evaluated using RMSD (Table 6).

In the absence of ligands, the protein exhibited RMSD fluctuations around an average of 0.26 nm. Upon binding of analogs, there was a slight decrease in RMSD values from 0.22 to 0.24 nm, indicating minor alterations in protein conformation upon complex formation. Lower RMSD values indicate stronger protein structures. RMSF plots were analyzed for both ligand-free and ligand-bound states. Without ligands, the enzyme had an average RMSF of 0.13 nm. However, after ligand binding, the average RMSD values for engeletin, ciprofloxacin, and griseofulvin slightly changed to 0.13, 0.12, and 0.14 nm, respectively, indicating stability of the complexes during simulation. The Rg offers insights into protein structural compactness, with smaller Rg values suggesting more compact protein structures. In complex formations, the average Rg values mostly remained unchanged or slightly decreased (Figure 1), suggesting that ligand binding minimally altered the structural compactness of tyrosine phosphatase. SASA measured the surface area of compounds accessible to solvent molecules. The mean SASA measurements for bioactive compounds remained nearly constant upon binding to tyrosine phosphatase, suggesting that the protein underwent conformational changes at a relatively slow rate and did not attain equilibrium, as evidenced by its solvent accessibility. Overall, the analysis indicates that equilibrium was not reached for this target during the 500 ns MD simulations.

Table 6. The mean values of RMSD, RMSF, Rg, and SASA over the entire 500 ns of MD simulations for the FtsZ protein

Complex	Mean RMSD (nm)	Mean RMSF (nm)	Mean Rg (nm)	Mean SASA (nm^2)
Engeletin + FtsZ	0.24	0.13	1.99	140.07
Ciprofloxacin + FtsZ	0.21	0.12	1.97	137.05
Griseofulvin + FtsZ	0.21	0.12	1.97	138.44
protein FtsZ	0.25	0.13	1.94	137.05

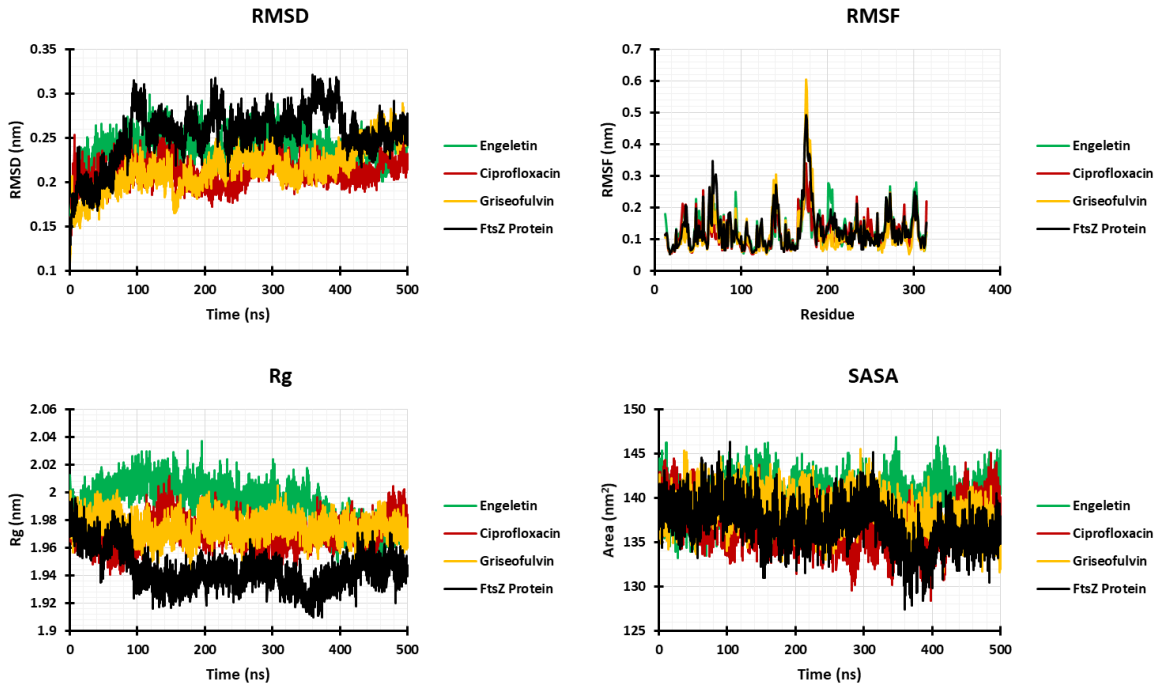

Figure 1. The dynamic structure of the ftsZ protein, the root means square deviation, root mean square fluctuations, the plot of radius of gyration, and the solvent-accessible surface area

The structural changes in tyrosine phosphatase (4R0T)

Molecular dynamics simulations were performed to investigate interactions between protein tyrosine phosphatase and bioactive compounds from *Petiveria alliacea* L., with complex stability assessed via RMSD (Table 7). The ligand-free protein showed RMSD fluctuations around 0.26 nm, while ligand-bound complexes exhibited slightly lower RMSDs (0.22–0.24 nm), indicating minor conformational changes and stable protein structures. RMSF analysis showed average fluctuations of 0.13 nm for the free enzyme, with

Table 7. The mean values of RMSD, RMSF, Rg, and SASA over the course of 500 ns of MD simulations for tyrosine phosphatase

Complex	Mean RMSD (nm)	Mean RMSF (nm)	Mean Rg (nm)	Mean SASA (nm^2)
Engeletin + Tyrosine phosphatase	0.24	0.13	1.51	83.94
Ciprofloxacin + Tyrosine phosphatase	0.22	0.12	1.50	82.90
Griseofulvin + Tyrosine Phosphatase	0.24	0.14	1.50	85.29
Protein tyrosine phosphatase	0.26	0.13	1.50	84.24

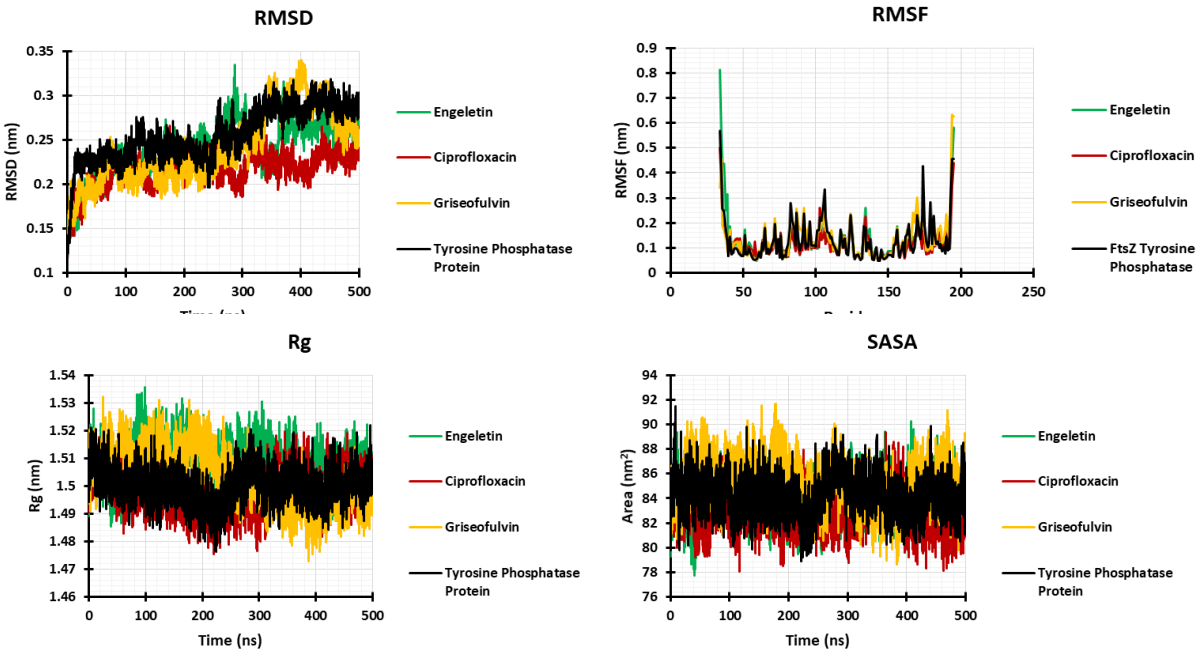

Figure 2. The dynamic structure of the tyrosine phospatase protein, the root means square deviation, root mean square fluctuations, the plot of radius of gyration, and the solvent-accessible surface area

slight changes upon binding engeletin, ciprofloxacin, and griseofulvin (0.12–0.14 nm), confirming complex stability. The radius of gyration (Rg) remained mostly unchanged or slightly decreased (Figure 2), suggesting minimal impact on protein compactness. SASA values of bound compounds were nearly constant, indicating slow conformational changes and that equilibrium was not reached during the 500 ns simulation.

Computational binding free energy calculations using MM-PBSA

The binding free energy at 500 ns was determined using the MM-PBSA method implemented in GROMACS 2016.3, analyzing the molecular dynamics data (Table 8). This involved computing the total binding free energy considering various factors like van der Waals interactions (ΔEVDW), electrostatic interactions (ΔEEEL), contributions from the Generalized Born method (ΔEGB), nonpolar solvation (ΔESURF), gas phase molecular mechanics energy (ΔGGAS), and solvation energy (ΔGSOLV) for the six complexes [44]. The total binding energies ranged between −74.004 and −126.107 kJ/mol (for FtsZ) and −10.684 and −45.855 kJ/mol (for tyrosine phosphatase), as detailed in Table 8. Furthermore, all MM-PBSA calculations indicated the formation of stable complexes between the six compounds and the active sites of the protein macromolecules, consistent with docking studies. The estimation of binding free energy supported the results obtained from molecular docking and dynamics simulations. Notably, engeletin exhibited substantially higher MM-PBSA binding free energy for both FtsZ and tyrosine phosphatase proteins compared to ciprofloxacin and griseofulvin during the 500 ns simulation. These findings hold promise for the development of effective drugs targeting infectious diseases.

Table 8. The components of binding energy computed using the MM-PBSA method

Complex	ΔEVDW (kJ/mol)	ΔEEEL (kJ/mol)	ΔEGB (kJ/mol)	ΔESURF (kJ/mol)	ΔGGAS (kJ/mol)	ΔGSOLV (kJ/mol)	ΔTOTAL (kJ/mol)
Engeletin + FtsZ	−211.027	−76.523	181.468	−20.025	0.000	0.000	−126.107
ciprofloxacin + FtsZ	−138.503	−35.580	115.316	−15.237	0.000	0.000	−74.004
Griseofulvin + FtsZ	−135.726	−0.561	67.886	−14.937	0.000	0.000	−83.338
Engeletin + Tyrosine phosphatase	−78.162	−6.042	47.050	−8.701	0.000	0.000	−45.855
Ciprofloxacin + Tyrosine phosphatase	−37.404	−23.135	53.962	−4.108	0.000	0.000	−10.684
Griseofulvin + Tyrosine phosphatase	−91.032	−98.468	184.981	−12.886	0.000	0.000	−17.406

Table 9. The components of binding energy computed using the MM-PBSA method

Microorganism	Phytochemical compound	Result	
		MIC (µg/mL)	MBC (µg/mL)
Staphylococcus aureus	Beta-sitosterol	6.25	6.25
	myricetin	7.5	7.5
Pseudomonas aeruginosa	Beta-sitosterol	1.5625	1.5625
	myricetin	3.25	3.25
Malassezia furfur	Beta-sitosterol	25	25
	myricetin	0.8125	3.25
Trichophyton mentagrophytes	Beta-sitosterol	12.5	12.5
	myricetin	7.5	7.5

In vitro antibacterial activity testing using the microdilution method

The antimicrobial activity of selected compounds is summarized in Table 9. Beta-sitosterol showed MIC and MBC values of 6.25 µg/mL against *Staphylococcus aureus*, while myricetin exhibited values of 7.5 µg/mL, indicating strong activity against this Gram-positive bacterium. Against *Pseudomonas aeruginosa*, beta-sitosterol was highly potent (MIC and MBC = 1.5625 µg/mL), and myricetin showed values of 3.25 µg/mL. These results suggest that beta-sitosterol exerts both bacteriostatic and bactericidal effects, likely due to its ability to penetrate the Gram-negative outer membrane, while myricetin also displays significant activity. Overall, both compounds are promising candidates against bacterial infections, particularly those caused by antibiotic-resistant *Pseudomonas aeruginosa*.

For antifungal activity, beta-sitosterol showed MIC and MBC values of 25 µg/mL against *Malassezia furfur*, whereas myricetin was more potent (MIC = 0.8125 µg/mL; MBC = 3.25 µg/mL). Against *Trichophyton mentagrophytes*, beta-sitosterol and myricetin had MIC and MBC values of 12.5 µg/mL and 7.5 µg/mL, respectively, indicating moderate to strong activity. Myricetin's superior efficacy is likely due to its higher polarity and multiple hydroxyl groups, which enhance interaction with fungal membranes, while beta-sitosterol's nonpolar structure and single hydroxyl group may limit its activity. Both compounds appear to act by disrupting fungal cell membranes or inhibiting

key enzymes, highlighting their potential as dual-action antimicrobial agents and promising candidates for broad-spectrum antimicrobial therapies.

Conclusion

This study focused on designing and evaluating the antibacterial activity of bioactive compounds derived from *Petiveria alliacea* L. using a combination of *in vitro* and computational approaches. The compounds' uniqueness in terms of antibacterial activity was confirmed through a search on the Clarivate Analytics Integrity portal. Molecular docking and PASS server predictions revealed strong binding affinities of the bioactive compounds toward the FtsZ protein and tyrosine phosphatase, key bacterial targets. Molecular dynamics simulations further validated the stability of the protein-ligand complexes, demonstrating their ability to induce significant conformational changes in the FtsZ protein and tyrosine phosphatase during the simulation. Engeletin, in particular, exhibited exceptional stability within the active site of tyrosine phosphatase, as evidenced by reduced RMSD and increased SASA values, highlighting its capacity to alter protein conformation upon binding. Similarly, MD simulations showed the remarkable stability of engeletin when interacting with FtsZ, with consistent RMSD, RMSF, Rg, and SASA values supporting its potential as a robust antibacterial agent. The integration of *in vitro* antibacterial activity testing provided experimental validation for the computational findings. Results from MIC and MBC assays confirmed the effectiveness of selected compounds in inhibiting and killing bacterial strains, thereby reinforcing their potential as antibacterial agents. These findings align with the computational predictions and emphasize the significance of FtsZ as a key bacterial target, considering its functional role as a prokaryotic homolog of eukaryotic microtubules targeted by griseofulvin. Ciprofloxacin's observed activity on tyrosine phosphatase also highlighted its versatile antibacterial potential, albeit dependent on specific cell types and conditions. While the number of compounds designed in this study was limited, the findings underscore the potential of hybridization approaches to enhance antibacterial activity. This work not only provides insights into the development of novel antibacterial compounds, but also establishes a robust framework for future research targeting bacterial proteins to create promising antibacterial agents.

Acknowledgments

The authors would like to express their sincere gratitude to the Faculty of Pharmacy, Universitas Bhakti Kencana, for the facilities, administrative support, and encouragement provided during the completion of this study.

Conflict of Interest

The authors declare that there is no conflict of interest regarding the publication of this manuscript.

ORCID

Jajang Japar Sodik
https://orcid.org/0009-0000-1156-1549
Entris Sutrisno
https://orcid.org/0000-0003-3830-6411
Dieni Mardliyani
https://orcid.org/0009-0008-1739-5375
Taufik Muhammad Fakih
https://orcid.org/0000-0001-7155-4412

References

[1] Dadgostar, P. Antimicrobial resistance: Implications and costs. *Infection and Drug Resistance*, **2019**, 3903-3910.

[2] Lalchhandama, K. History of penicillin. *WikiJournal of Medicine*, **2021**, 8(1), 1-16.
[3] Banani, H., Marcet-Houben, M., Ballester, A.-R., Abbruscato, P., González-Candelas, L., Gabaldón, T., Spadaro, D. Genome sequencing and secondary metabolism of the postharvest pathogen penicillium griseofulvum. *BMC Genomics*, **2016**, 17(1), 19.
[4] Liang, Y., Zhang, B., Li, D., Chen, X., Wang, Q., Shu, B., Li, Q., Tong, Q., Chen, C., Zhu, H. Griseofulvin analogues from the fungus penicillium griseofulvum and their anti-inflammatory activity. *Bioorganic Chemistry*, **2023**, 139, 106736.
[5] Ramesh, M., Sujitha, M., Anila, P.A., Ren, Z., Poopal, R.K. Responses of cirrhinus mrigala to second-generation fluoroquinolone (ciprofloxacin) toxicity: Assessment of antioxidants, tissue morphology, and inorganic ions. *Environmental Toxicology*, **2021**, 36(5), 887-902.
[6] Zhang, G.F., Liu, X., Zhang, S., Pan, B., Liu, M.L. Ciprofloxacin derivatives and their antibacterial activities. *European Journal of Medicinal Chemistry*, **2018**, 146, 599-612.
[7] Kashyap, A., Singh, P.K., Silakari, O. Chemical classes targeting energy supplying gyrb domain of mycobacterium tuberculosis. *Tuberculosis*, **2018**, 113, 43-54.
[8] Kerdudo, A., Gonnot, V., Njoh Ellong, E., Boyer, L., Michel, T., Adenet, S., Rochefort, K., Fernandez, X. Essential oil composition and biological activities of *Petiveria alliacea* l. From martinique. *Journal of Essential Oil Research*, **2015**, 27(3), 186-196.
[9] Kim, S., Kubec, R., Musah, R.A. Antibacterial and antifungal activity of sulfur-containing compounds from *Petiveria alliacea* l. *Journal of Ethnopharmacology*, **2006**, 104(1-2), 188-192.
[10] Ochoa Pacheco, A., Marín Morán, J., González Giro, Z., Hidalgo Rodríguez, A., Mujawimana, R.J., Tamayo González, K., Sariego Frómeta, S. In vitro antimicrobial activity of total extracts of the leaves of *Petiveria alliacea* l.(anamu). *Brazilian Journal of Pharmaceutical Sciences*, **2013**, 49, 241-250.
[11] Mulyani, Y., Sukandar, E., Adyana, I. Aktivitas anti bakteri singawalang (*Petiveria alliaceae*) terhadap bakteri yang resisten dan peka terhadap antibiotik. *Bionatura*, **2012**, 14(1).
[12] Mathur, H., Field, D., Rea, M.C., Cotter, P.D., Hill, C., Ross, R.P. Fighting biofilms with lantibiotics and other groups of bacteriocins. *NPJ Biofilms and Microbiomes*, **2018**, 4(1), 9.
[13] Church, N.A., McKillip, J.L. Antibiotic resistance crisis: Challenges and imperatives. *Biologia*, **2021**, 76(5), 1535-1550.
[14] Myrko, I., Chaban, T., Demchuk, Y., Drapak, Y., Chaban, I., Drapak, I., Pankiv, M., Matiychuk, V. Current trends of chemoinformatics and computer chemistry in drug design: A review. *Current Chemistry Letters*, **2024**, 13(1), 151-162.
[15] Ahmad, S., Raza, S., Uddin, R., Azam, S.S. Comparative subtractive proteomics-based ranking for antibiotic targets against the dirtiest superbug: Acinetobacter baumannii. *Journal of Molecular Graphics and Modelling*, **2018**, 82, 74-92.
[16] Song, D., Zhang, N., Zhang, P., Zhang, N., Chen, W., Zhang, L., Guo, T., Gu, X., Ma, S. Design, synthesis and evaluation of novel 9-arylalkyl-10-methylacridinium derivatives as highly potent ftsz-targeting antibacterial agents. *European Journal of Medicinal Chemistry*, **2021**, 221, 113480.
[17] Geronikaki, A., Kartsev, V., Petrou, A., Akrivou, M., Vizirianakis, I., Chatzopoulou, F.M., Lichitsky, B., Sirakanyan, S., Kostic, M., Smiljkovic, M. Antibacterial activity of griseofulvin analogues as an example of drug repurposing. *International Journal of Antimicrobial Agents*, **2020**, 55(3), 105884.
[18] Paul, N.M., Yoder, R.J., Callam, C.S. Incorporating chemical structure drawing software throughout the organic laboratory curriculum. *Journal of Chemical Education*, **2019**, 96(11), 2638–2642.
[19] Chen, I.J., Foloppe, N. Drug-like bioactive structures and conformational coverage with the LigPrep/ConfGen suite: Comparison to programs MOE and Catalyst. *Journal of Chemical Information and Modeling*, **2010**, 50(5), 822-839.
[20] Xu, K., Li, S., Yang, W., Li, K., Bai, Y., Xu, Y., Jin, J., Wang, Y., Bartlam, M. Structural and biochemical analysis of tyrosine phosphatase related to biofilm formation a (tpba) from the opportunistic pathogen pseudomonas aeruginosa pao1. *PLoS One*, **2015**, 10(4), e0124330.
[21] Matsui, T., Yamane, J., Mogi, N., Yamaguchi, H., Takemoto, H., Yao, M., Tanaka, I. Structural reorganization of the bacterial cell-division protein ftsz from staphylococcus aureus. *Biological Crystallography*, **2012**, 68(9), 1175-1188.
[22] Skarzynski, T., Mistry, A., Wonacott, A., Hutchinson, S.E., Kelly, V.A., Duncan, K. Structure of udp-n-acetylglucosamine enolpyruvyl transferase, an enzyme essential for the synthesis of bacterial peptidoglycan, complexed with substrate udp-n-acetylglucosamine and the drug fosfomycin. *Structure*, **1996**, 4(12), 1465-1474.
[23] Lim, D., Strynadka, N.C. Structural basis for the β lactam resistance of pbp2a from methicillin-resistant staphylococcus aureus. *Nature structural biology*, **2002**, 9(11), 870-876.
[24] Stanger, F.V., Dehio, C., Schirmer, T. Structure of the n-terminal gyrase b fragment in complex with ADP· PI reveals rigid-body motion induced by ATP hydrolysis. *PLoS One*, **2014**, 9(9), e107289.

[25] Bellon, S., Parsons, J.D., Wei, Y., Hayakawa, K., Swenson, L.L., Charifson, P.S., Lippke, J.A., Aldape, R., Gross, C.H. Crystal structures of escherichia coli topoisomerase iv pare subunit (24 and 43 kilodaltons): A single residue dictates differences in novobiocin potency against topoisomerase iv and DNA gyrase. *Antimicrobial Agents and Chemotherapy*, **2004**, 48(5), 1856-1864.
[26] Keck, J.L., Roche, D.D., Lynch, A.S., Berger, J.M. Structure of the RNA polymerase domain of e. Coli primase. *Science*, **2000**, 287(5462), 2482-2486.
[27] Lagunin, A., Stepanchikova, A., Filimonov, D., Poroikov, V. Pass: Prediction of activity spectra for biologically active substances. *Bioinformatics*, **2000**, 16(8), 747-748.
[28] Eberhardt, J., Santos-Martins, D., Tillack, A.F., Forli, S. Autodock vina 1.2. 0: New docking methods, expanded force field, and python bindings. *Journal of Chemical Information and Modeling*, **2021**, 61(8), 3891-3898.
[29] Forli, W., Halliday, S., Belew, R., Olson, A. Autodock version 4.2. Citeseer, **2012**.
[30] Tian, W., Chen, C., Liang, J. CASTP 3.0: Computed atlas of surface topography of proteins and beyond. *Biophysical Journal*, **2018**, 114(3), 50a.
[31] Chen, F., Sun, H., Wang, J., Zhu, F., Liu, H., Wang, Z., Lei, T., Li, Y., Hou, T. Assessing the performance of MM/PBSA and MM/GBSA methods. 8. Predicting binding free energies and poses of protein–RNA complexes. *RNA*, **2018**, 24(9), 1183-1194.
[32] Systèmes, D. Dassault systèmes biovia, discovery studio modeling environment. *Dassault Systèmes Biovia, Discovery Studio Modeling Environment*, **2017**.
[33] Aho, N., Buslaev, P., Jansen, A., Bauer, P., Groenhof, G., Hess, B. Scalable constant pH molecular dynamics in GROMACS. *Journal of Chemical Theory and Computation*, **2022**, 18(10), 6148–6160.
[34] Abraham, M.J., Murtola, T., Schulz, R., Páll, S., Smith, J.C., Hess, B., Lindahl, E. GROMACS: High performance molecular simulations through multi-level parallelism from laptops to supercomputers. *SoftwareX*, **2015**, 1, 19-25.
[35] Kagami, L., Wilter, A., Diaz, A., Vranken, W. The ACPYPE web server for small-molecule md topology generation. *Bioinformatics*, **2023**, 39(6), btad350.
[36] Genheden, S., Ryde, U. The MM/PBSA and MM/GBSA methods to estimate ligand-binding affinities. *Expert Opinion on Drug Discovery*, **2015**, 10(5), 449-461.
[37] Elshikh, M., Ahmed, S., Funston, S., Dunlop, P., McGaw, M., Marchant, R., Banat, I.M. Resazurin-based 96-well plate microdilution method for the determination of minimum inhibitory concentration of biosurfactants. *Biotechnology Letters*, **2016**, 38(6), 1015-1019.
[38] Golus, J., Sawicki, R., Widelski, J., Ginalska, G. The agar microdilution method–a new method for antimicrobial susceptibility testing for essential oils and plant extracts. *Journal of applied microbiology*, **2016**, 121(5), 1291-1299.
[39] Kuban-Jankowska, A., Kostrzewa, T., Gorska-Ponikowska, M. Bacterial protein tyrosine phosphatases as possible targets for antimicrobial therapies in response to antibiotic resistance. *Antioxidants*, **2022**, 11(12), 2397.
[40] Santana-Molina, C., Saz-Navarro, D.d., Devos, D.P. Early origin and evolution of the ftsz/tubulin protein family. *Frontiers in Microbiology*, **2023**, 13, 1100249.
[41] Zhang, Y., Giurleo, D., Parhi, A., Kaul, M., Pilch, D.S., LaVoie, E.J. Substituted 1, 6-diphenylnaphthalenes as ftsz-targeting antibacterial agents. *Bioorganic & Medicinal Chemistry Letters*, **2013**, 23(7), 2001-2006.
[42] Xin, L., Hu, Z., Han, R., Xu, X., Wang, C., Li, D., Guo, Y., Hu, F. Asp50Glu mutation in MurA results in fosfomycin resistance in enterococcus faecium. *Journal of Global Antimicrobial Resistance*, **2022**, 30, 50-55.
[43] Usia, T., Iwata, H., Kadota, S., Tezuka, Y. Mechanism-based inhibition of CYP3A4 AND CYP2D6 by indonesian medicinal plants. *Journal of Ethnopharmacology*, **2006**, 105(3), 449-455.
[44] Aulifa, D.L., Al Shofwan, A.A., Megantara, S., Fakih, T.M., Budiman, A. Elucidation of molecular interactions between drug–polymer in amorphous solid dispersion by a computational approach using molecular dynamics simulations. *Advances and Applications in Bioinformatics and Chemistry*, **2024**, 1-19.

HOW TO CITE THIS MANUSCRIPT
J.J. Sodik, E. Sutrisno, D. Mardliyani, T.M. Fakih. Uncovering Antibacterial Agents in *Petiveria alliacea* through Computational and Experimental Methods. *Asian Journal of Green Chemistry*, 10 (4) 2026, 601-627.
DOI: https://doi.org/10.48309/AJGC.2026.556397.1857
URL: https://www.ajgreenchem.com/article_238963.html